

How Does External Pressure Shape Li Dendrites in Li Metal Batteries?

Xin Shen, Rui Zhang, Peng Shi, Xiang Chen, and Qiang Zhang*

High-energy density lithium metal batteries have achieved great progress as next-generation rechargeable cells. However, the huge gap in the switching from coin to pouch cells hinders their practical application. External pressure, as one discrepancy between coin and pouch cells, plays an important role in the performance of Li metal anodes. Herein the mechanism for the impact of external pressure on Li dendrites is revealed and quantified by a mechano-electrochemical phase field model. Two influence approaches are outlined as: 1) Inhibiting the progress of electroplating reactions, which lower the rate performance of cells; 2) Shaping the morphology of Li dendrites to be smooth and dense but increasing the mechanical instability. Furthermore, a phase diagram of routine electrolytes (including electrolyte-immersed separators and solid polymer electrolytes) with respect to various external pressures is established, giving rational guidance for designing pressure management systems in working batteries.

separator can be pierced by Li dendrites, further resulting in a short circuit and safety hazard.^[5]

There is remarkable progress on material advancement (including interface optimization,^[6] functional frameworks,^[7] as well as liquid and solid electrolyte innovation^[8]) to suppress Li dendrites and enhance the performance of Li metal anodes. For instance, Zhang et al. proposed a strategy of sustainable solid electrolyte interphase (SEI), successfully realizing a long cycle life of over 150 cycles (80% capacity retains) while only four cycles with pristine SEI in Li metal coin cells under practical conditions.^[9] However, there is a huge decline in the switching from coin to pouch cells (60 cycles). Therefore, it is necessary and urgent to bridge the gap between the

1. Introduction

Lithium (Li) metal is receiving growing interest as the high-energy density anode alternative to graphite due to its ultra-high theoretical capacity (3860 mAh g⁻¹) and extremely low redox potential (-3.04 V versus standard hydrogen electrode);^[1] Li metal batteries with a leap forward energy density of over 400 Wh kg⁻¹, such as Li-S and Li-O₂ batteries, are highly expected to be the next-generation rechargeable batteries.^[2] However, the practical demonstration of Li metal anodes is still challenging. In particular, disastrous Li dendrites blown by the large surface self-diffusion barrier of Li are uncontrollable, pointing to an inherent limitation.^[3] Its high specific surface area and high reactivity further cause copious irreversible side reactions and dead Li, eventually shortening the cell life and deteriorate the Coulombic efficiency.^[4] Even worse, a

coin and pouch cell, i.e., laboratory prototypes and practical applications.^[10]

One of the discrepancies between coin and pouch cells is the stress state. In detail, there is a volume expansion during the cycling of Li metal anodes, stemming from the accumulation of dendritic or inactive Li. An average thickness increase rate of 1.2 μm mAh⁻¹ exists in a Li|Li symmetric cell cycled at 5 mA cm⁻² and 1 mAh cm⁻² according to the report by He and co-workers.^[11] Such thickness variation further converts into stress accumulation for the coin cell due to the space constraint derived from the rigid steel shell. In contrast, little stress is accumulated for the pouch cell encapsulated by the soft aluminium-plastic film during repeated cycles. Then what happens under different stress states? Taking Li|Cu pouch cell as a model system and applying external pressures for achieving stress accumulation, there is a shift from a loose and porous electroplated morphology to a smooth and dense morphology after applying the external pressure (**Figure 1a–d**). Furthermore, the Coulombic efficiency (CE) and cycle life are both improved by the applied external pressure (**Figure 1e,f**). Hence, it is necessary to find the optimal pressure and employ a pressure management system for overcoming the gap between coin and pouch cells.^[12]

In spite of massive screening experiments for optimizing pressure,^[13] it is unclear that why and how external pressure can shape Li dendrites and improve the performance of Li metal batteries. As experimental method is difficult to measure the stress evolution in situ in a cell, theoretical analysis and quantitative simulation are favored. Generally, there are two states that should be considered for explaining the impact of external

X. Shen, P. Shi, Dr. X. Chen, Prof. Q. Zhang
Beijing Key Laboratory of Green Chemical Reaction
Engineering and Technology
Department of Chemical Engineering
Tsinghua University
Beijing 100084, China
E-mail: zhang-qiang@mails.tsinghua.edu.cn

Dr. R. Zhang
Advanced Research Institute of Multidisciplinary Science
Beijing Institute of Technology
Beijing 100081, China

 The ORCID identification number(s) for the author(s) of this article can be found under <https://doi.org/10.1002/aenm.202003416>.

DOI: 10.1002/aenm.202003416

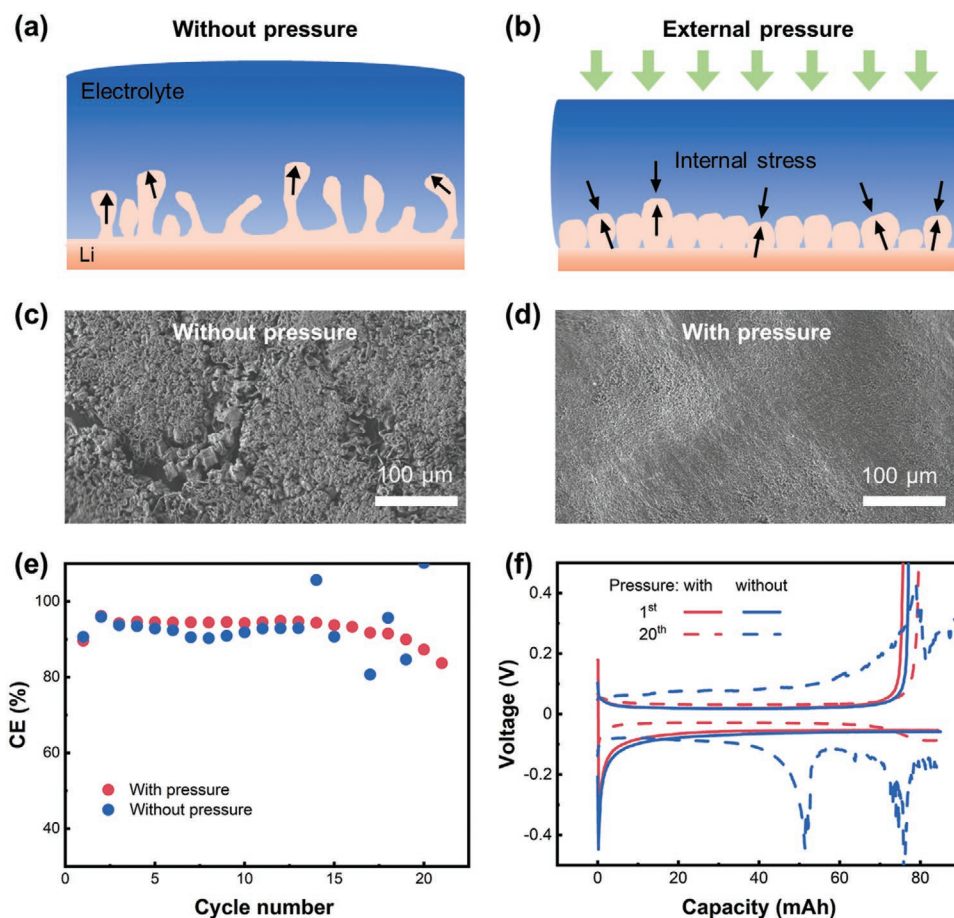


Figure 1. The impact of external pressure on Li metal anodes. Schematic illustration of the morphology of Li dendrites a) without and b) with external pressure. Scanning electron microscope (SEM) images of Li electroplated morphology c) without and d) with external pressure. Electrochemical performance of Li|Cu pouch cells, e) Coulombic efficiency, and f) corresponding polarization curves at a current density of 1.0 mA cm^{-2} with a capacity of 3.0 mAh cm^{-2} . The application of external pressure remarkably shapes the morphology and improves the performance of Li metal anodes.

pressure: 1) Steady state, such as packing and rest. In this respect, mechanical deformation (elastic, plastic deformation and creep) is the only impact induced by external pressure.^[14] Especially, the interface contacts can be significantly enhanced by applying external pressure, and thus improves the cell performance (Figure S1, Supporting Information).^[15] 2) Dynamic state, in which the cell is under cycling. There is a complicated coupling of mechanics, electrochemical reaction, and ion transport in this state. Thanks to the development of computational studies, abundant computational methods ranging from atomistic scale to the continuum level have offered insights into the Li electrodeposition morphology, such as smoothed particle hydrodynamics method,^[16] coarse-grained Monte Carlo method,^[17] phase field,^[18] level set,^[19] and deformed mesh.^[20] The developed mechano-electrochemical theory can well explain the relationship between internal stress and electrochemical reaction.^[21] Most notably, Neman and co-workers proposed that a polymer electrolyte with a shear modulus which is about twice that of Li can suppress Li dendrites.^[22] Yet the impact of external pressure during cycling needs to be further discussed.

In this contribution, a mechano-electrochemical phase field model was employed to describe the electroplating evolution in response to the external pressure. With a systematic analysis of the internal stress distribution induced by external pressure

and the resultant dendrite morphology, the impacts of external pressure on electroplating are outlined as: 1) Inhibiting the progress of electroplating reaction; 2) Shaping the morphology of Li dendrites to be smooth and dense but enlarging the mechanical instability. Furthermore, a diagram for quantifying the effect of dendrite suppression under various external pressures in common electrolyte circumstances (e.g., electrolyte-immersed polypropylene (PP) separator) is established. This provides a rational basis to design favorable external pressure in packing and operation, promoting the practical applications of Li metal anodes in pouch cells.

2. Results and Discussion

2.1. Mechano-Electrochemical Phase Field Model

A mechano-electrochemical phase field model was proposed to reproduce the multiphysics processes in the Li|Cu half cell. The two-dimensional domain (Figure S2, Supporting Information) employed herein consists of an electrode with a Li metal nucleation site and electrolyte. The electrolyte represents liquid electrolyte immersed separator or solid polymer electrolyte and its elastic modulus is set as 1.0 GPa without additional

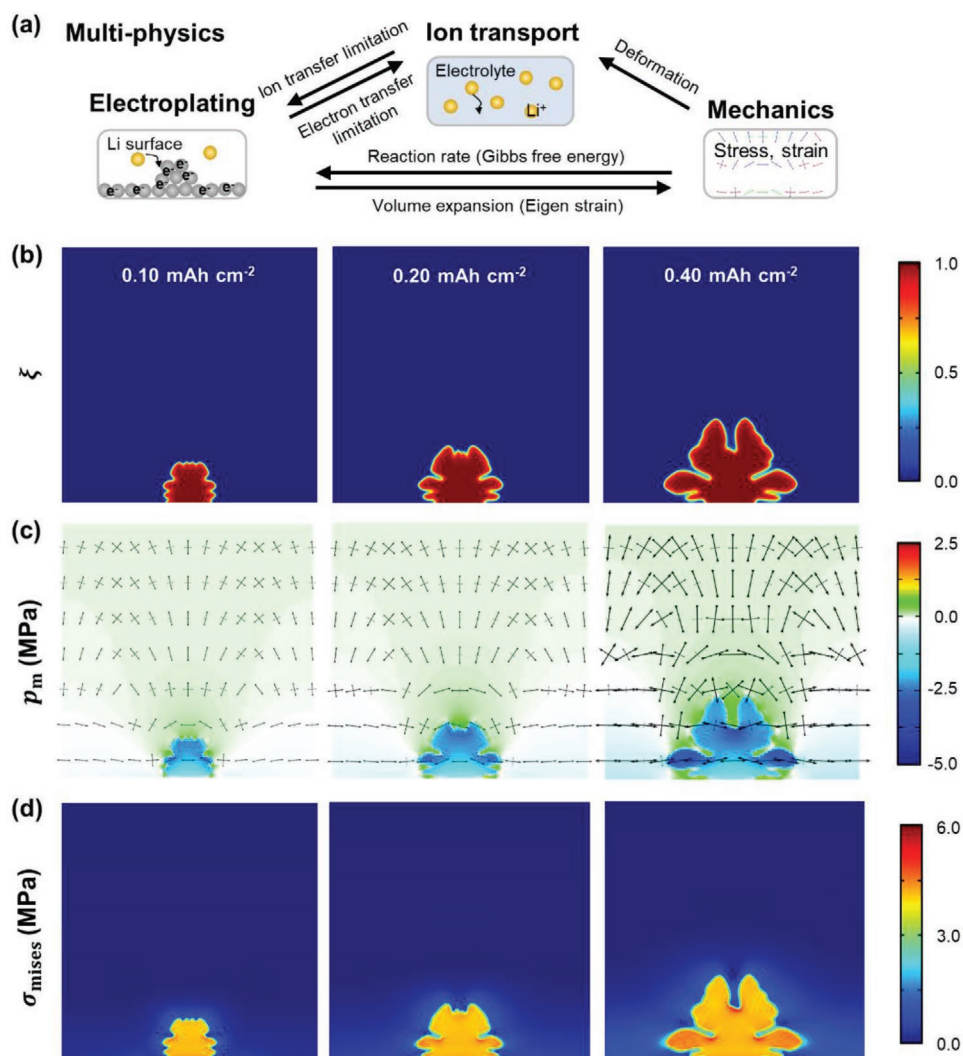


Figure 2. Mechano-electrochemical phase field model. a) Schematic illustration of multiphysics in Li metal batteries. b–d) The simulated results of Li dendrites in the absence of external pressure at selected plating capacity of 0.10, 0.20, and 0.40 mAh cm⁻². Specifically, b) dendritic morphology, c) principle stress, and hydrostatic pressure, and d) von Mises stress evolution. In (c), the arrow head orientation represents the principal stress direction and the length is a measurement. Besides, the negative hydrostatic pressure denotes tensile regions while the positive hydrostatic pressure represents compressive regions. Above snapshots are captured from the Videos S1 (Supporting Information).

explanation. The computational domain is a half cell (including an anode and half of electrolyte layer), i.e., the opposite cathode where Li stripping reaction occurs is ignored. The top boundary of electrolyte is assumed as the bulk solution with a constant concentration. This configuration is able to reflect the realistic physical fields nearby the anode in Li|Cu half cells or Li|Li symmetric cells meanwhile it rationally simplifies the model. We assume that, since the electrolyte is flowable or deformable, Li/electrolyte interface is perfect contact after cell package. A constant voltage of 0.10 V was applied as a driving force. **Figure 2a** illustrates the physical coupling between electroplating, ion transport, and mechanics in this model. Once the voltage is applied on the cell, the electrochemical reaction of $\text{Li}^+ + \text{e}^- \rightarrow \text{Li}$ occurs, leading to the subsequent dynamic response. The classical competition between ion and electron on the Li surface has been discussed for electroplating and ion transport in

our previous work.^[23] With regard to mechanics and electroplating, the mechanical response in the form of Eigen strain is triggered by electroplating, while the reaction rate is subject to the mechanical energy (included in Gibbs free energy) in turn.^[24] Besides, local deformation can give rise to the ion redistribution. Above complicated process results in the diverse morphology of Li dendrites, which remarkably determines the performance of Li metal anodes.

Detailed simulation methods are given in the Experimental Section. The kernel is to introduce an order parameter ξ for describing the two phase and construct an energy variational approach for driving the modeling system. In particular, $\xi = 1$ denotes the Li metal electrode and $\xi = 0$ represents the electrolyte. Taking into account the high yield strength of Li dendrites,^[25] the Li metal and electrolyte are both treated as linear elastic materials for simplification.

The Li dendrite growth in the absence of external pressure was first simulated by this mechano-electrochemical phase field model (Video S1, Supporting Information). The size of visualized domain is $20 \times 20 \mu\text{m}$ and it remains the same for all other snapshots and videos hereafter. As the electroplating proceeds, the nucleation site grows into a branching morphology owing to the specific crystallographic orientation of Li (bcc) (Figure 2b). Meanwhile, the strong electric field concentrated on the dendrite tips further accelerates forked plating and vertical growth. The corresponding Li^+ concentration (c_{Li^+}), electrostatic potential (ϕ), electric field intensities, and local current density distribution (i_{loc}) are presented in Figure S3 (Supporting Information), respectively. On the other hand, the electrolyte is compressed and deformed because of the penetration of Li dendrites. The principle stress, hydrostatic pressure, and von Mises stress are employed for visualizing mechanical response of Li and electrolyte. Figure 2c exhibits the distribution of principle stress and hydrostatic pressure (p_m). The former describes the stress tensor distribution and the latter purely corresponds to the uniaxial stresses. The volumetric change of the cell is well exhibited (negative value denotes tensile state and positive value represents compressive state) from the distribution of hydrostatic pressure. In the absence of external pressure (or space confinement), the cell is able to free expansion for releasing partial stress. Therefore, the hydrostatic pressure on the up and down edges is smaller than the Li/electrolyte interfaces. Figure 2d shows the distribution of von Mises stress (σ_{mises}), indicating the probability of plastic yielding, i.e., distorting the shape of the material. Evidently, it is highly concentrated on the bifurcations of Li dendrites. Theoretically kinks are preferred to form in these sites. However, the maximum von Mises herein is no more than 6.0 MPa, which is less than the yield strength of

Li dendrites (it increases from 15.0 to 105.0 MPa as the dendrite diameter decreases from 9.45 to $1.39 \mu\text{m}$).^[25b] Therefore, the hypothesis of Li treated as the linear elastic matter is rational.

In spite of the internal stress generated by the cell itself, the Li dendrite is unable to be suppressed in electrolyte-immersed separator or solid polymer electrolyte (denoted as “soft” electrolyte) without external pressure. Ren et al. has reported that when the elastic modulus of electrolyte is larger than 9.0 GPa, the dendrites can be partially suppressed.^[26] However, such a very high modulus is extremely difficult to reach in practical cells with polymer based electrolytes. It can be achieved only with inorganic solid-state electrolyte (such as garnet). Unfortunately, there is dendrite growth in inorganic solid-state electrolyte. However, there is an essential difference in the reason of failing to inhibit dendrites. In contrast to the “soft” electrolyte, inorganic solid-state electrolyte is so “hard” that poor interface contact and crack propagation becomes the main trouble.^[27] The improvement of material compactness and interface wettability is more important for “hard” electrolyte, while the external pressure is helpful for “soft” electrolyte.

2.2. Pressure-Shaped Li Dendrites

The Li dendrite growth under various external pressures is presented in Figure 3 and Video S2 (Supporting Information), and the corresponding evolution of electrochemical field can be found in Figure S4 (Supporting Information). All snapshots are captured with the same plating capacity of 0.4 mAh cm^{-2} . When the external pressure increases from 2.0 to 14.0 MPa, the morphology of Li dendrites tends to be relatively smooth with less branches (Figure 3a). As can be observed in Figure 3b, the

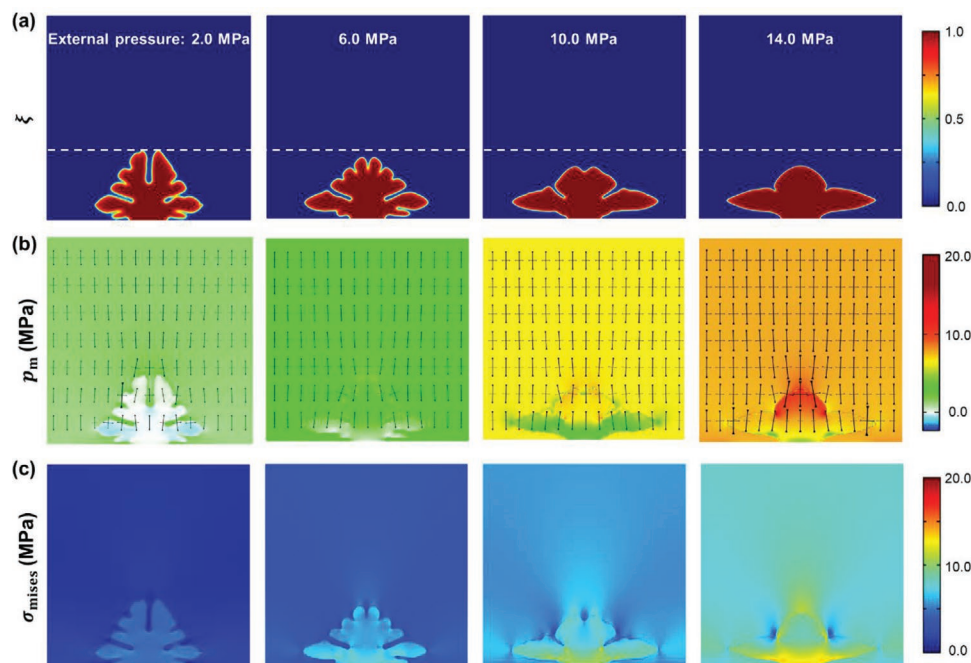


Figure 3. The simulated results of Li dendrites under the external pressure ranging from 2.0 to 14.0 MPa. The snapshots of a) dendritic morphology, b) principle stress and hydrostatic pressure, and c) von Mises stress evolution at a plating capacity of 0.4 mAh cm^{-2} . Increasing external pressure helps to smooth the dendrite morphology.

local hydrostatic pressure in the Li dendrites ranges from negative to positive value, i.e., shifts from expansion to compressive state while the applied external pressure is larger than the electrochemical eigen stress. Besides, there is maximum hydrostatic pressure in the tip of Li dendrites, which reaches up to 20.0 MPa at an external pressure of 14.0 MPa (Figure 3b). Therefore, tip growth is inhibited and lateral growth is promoted. Such smooth and stocky dendrite can significantly reduce the specific surface area and improve densification, which is consistent with the experimental results in Figure 1c,d.

However, it is worth noting that the applied external pressure also brings potential risks of material failure besides the benefits of the inhibition of dendrite growth. A conservative approach for determining the maximum allowable external pressure is to reference the yield strength of materials. Herein von Mises yield criterion is employed. Once the von Mises stress is over the yield strength, the polymer electrolyte is unable to rebound with the stripping of Li dendrites. Besides, the fracture of Li dendrites might further occur and convert into dead Li. These both induce the loss of electrical contacts between electrolyte and Li dendrites, and finally decline the Coulombic efficiency of cells. It is difficult to precisely determine the yield strength for various materials applied in a working cell. Therefore, the upper limit of external pressure is not given herein. The upper limit of external pressure can be probed by referencing the material properties. For instance, HY-6100 PP separator possesses a yield strength of ≈ 20.0 MPa (Table S1, Supporting Information). In addition, the location of maximum stress deserves attention. Figure 3c shows the distribution of

von Mises stress. With the increase of external pressure, the concentration of von Mises stress shifts from the bifurcations to the root of Li dendrite, and the maximum value increases from 5.8 to 19.5 MPa. In other words, the risk of root fracture is greatly increased, which can cause more serious decline of Coulombic efficiency than bifurcation fracture.

To further quantitatively understand the shape effect of external pressure, more results are extracted from the simulated data (Figure 4). The dependences of the electrochemical reaction on the external pressure are investigated from the plating timescales (Figure 4a,b). Herein the average current density is defined as an average value of the local current density. As the external pressure increases from 0 to 14.0 MPa, the average current density of the cell decreases (Figure 4a). Taking the plating time of 100 s for example, the plating capacity reduces from 0.51 to 0.41 mAh cm⁻², and the average current density decreases from 20.49 to 17.44 mA cm⁻² (Figure 4b). The reduction deviates from the linear law to a certain extent trend. Once the external pressure is less than 4.0 MPa, no obvious decrease of plating capacity and current density are observed.

The effect of external pressure on electrochemical reaction can be divided into three intervals and can be further understood mathematically by the contribution of mechanical driving force ($-f'_{\text{els}}(\mathbf{u}, \xi)$, see Model Formulation) in the driving force corresponded to interfacial energy ($-(g'(\xi) + f'_{\text{grad}}(\xi) + f'_{\text{els}}(\mathbf{u}, \xi))$, see Model Formulation): 1) No effect. The external pressure is so small that it is unable to remarkably change the distribution of internal stress, i.e., the mechanical driving force contributes little to the driving force of interfacial energy. 2) Linear

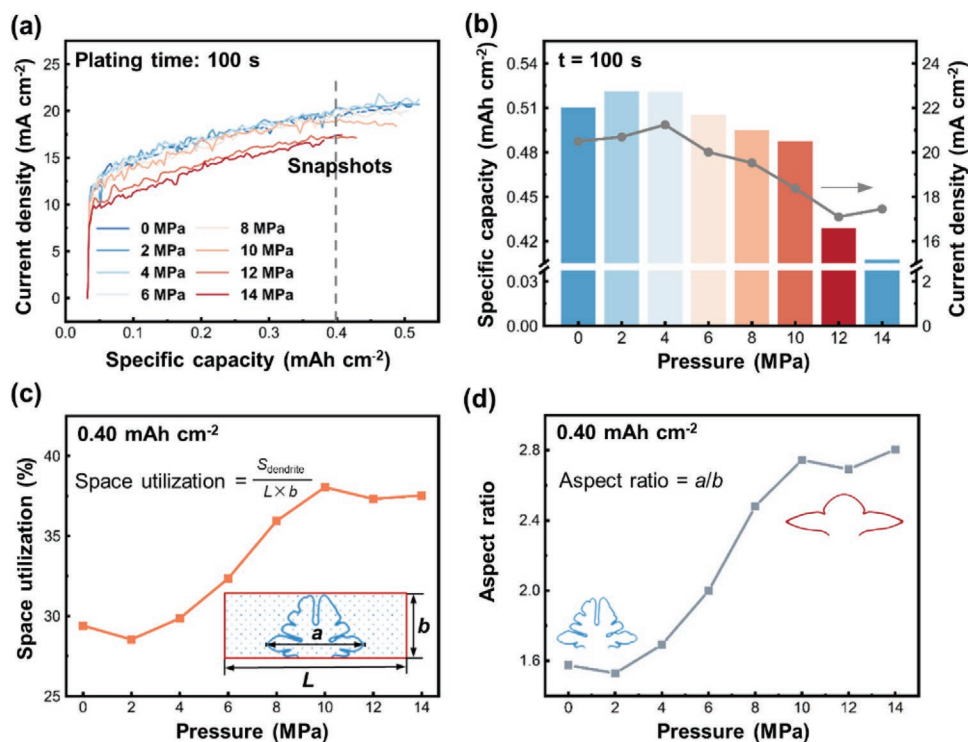


Figure 4. The analysis results of Li dendrites under the external pressure ranging from 0 to 14 MPa. a,b) The impact of external pressure on the progress of electroplating reactions. a) The current density versus the specific capacity. b) The current density and specific capacity at a plating time of 100 s. c,d) Morphology of Li dendrites with respect to external pressures. c) The space utilization and d) the aspect ratio at a plating capacity of 0.40 mAh cm⁻².

influence. The electrochemical reaction is linearly inhibited with increasing external pressure. The mechanical driving force dominates the driving force of interfacial energy, thus linearly slow down the reaction rate $\left(\frac{\partial \xi}{\partial t}\right)$. This inhibition effect brought about by external pressure is harmful to the rate performance of batteries. 3) Saturation. Internal stress gets extremely large due to the spatial confinement and the degree of material compression, i.e., the mechanical driving force hardly changes. Moreover, it can be inferred that when extended to the working condition of constant current, the dependences of the electrochemical reactions on the external pressure will be presented as the variation of overpotentials.

To quantify the effect of external pressure on plating morphology, the space utilization (U_s) and the aspect ratio (R_a) are defined as

$$U_s = \frac{S_{\text{dendrite}}}{L \times b} \quad (1)$$

$$R_a = a/b \quad (2)$$

where S_{dendrite} is the surface area of Li dendrite, L the width of the calculated domain, a and b the width and height of Li dendrite, respectively. U_s is a sign of densification and porosity of the Li metal electrode. The increase of U_s can qualitatively reflect the decrease of porosity and the increase of densification in a Li metal electrode. R_a reflects the shape of Li dendrite (slender or stocky). The space utilization and the aspect ratio at a plating capacity of 0.40 mAh cm^{-2} under different external pressures are exhibited in Figure 4c,d. When the external pressure increases from 2.0 to 10.0 MPa, the space utilization increases from 29.4% to 37.3% and the aspect ratio increases from 1.6 to 2.8. The electroplating morphology with a high space utilization and a high aspect ratio will be benefit for improving the utilization of electroplated Li and reducing the risk of short circuit.

In the case of multisite electroplating, the effect of external pressure on the Li dendrite growth exhibits similar results (Figure S5, Supporting Information). Due to the mutual extrusion between the dendrites, the growth in the lateral direction will be more restricted, resulting in high internal stress. In the absence of external pressure, the maximum value of hydrostatic pressure and von Mises stress can reach up to 10.0 and 14.0 MPa, respectively, more than twice the case of single site (Figure S5e and S5f, Supporting Information). Besides, the stress concentration at the root is more obvious, causing a huge instability (break). With the increase of external pressure, Li electroplated morphology becomes flat and electrochemical reaction is suppressed (Figure S5g and S5h, Supporting Information).

Collectively, the effect of external pressure on the Li dendrite growth mainly consists of two contents: 1) Inhibiting the progress of electroplating reaction, which is against the rate performance of cells. 2) Shaping the morphology of Li dendrites to be smooth but enlarging the mechanical instability. Therefore, moderate external pressure is advocated for improving the performance of Li metal anode.

It is noteworthy that the performance of Li metal anodes is also related to the stripping process. Although it is not

simulated herein, the previous research on corrosion science can give a reference. Gutman^[28] has derived the relationship between elastic deformation and equilibrium potential:

$$\Delta \phi_{\text{eq}} = \frac{p_m V_m}{zF} \quad (3)$$

where V_m represents the molar volume, z the number of charge, F the Faraday constant. According to the distribution of stress in Figures 2 and 3, it can be inferred that the external pressure will regulate the preferential stripping location, such as root-stripping and tip-stripping, thereby influences the Coulombic efficiency.

2.3. Electrolyte Variation

The pressure shaping effect on the Li dendrite growth in electrolytes of elastic moduli ranging from 0.5 to 2.0 GPa under a fixed external pressure of 6.0 MPa was further investigated (Figure 5a–c). It is observed that, the suppression effect on Li dendrite is more significant with a lower elastic modulus of electrolyte (Figure 5a). Comparing with Figure 3a, when a similar dendritic morphology is formed in the electrolyte with an elastic modulus of 0.5 GPa, it only needs an external pressure of 6.0 MPa, while in the electrolyte with an elastic modulus of 1.0 GPa, it needs an external pressure of 10.0 MPa. Further quantitative analysis was employed. In terms of the electrochemical reaction, only small variations are observed in Figure 5b. The internal stress reinforced by stiff electrolyte is inconspicuous. In terms of space utilization, U_s reduces from 38.8% to 28.5% with the electrolyte modulus increasing from 0.5 to 2.0 GPa (Figure 5c). In other words, applying external pressure is more effective for low modulus electrolyte systems. Notably, the elastic modulus of electrolyte discussed herein is lower than that of Li metal.

Extended results on combined effects of external pressure and electrolyte were incorporated in Figure 5d and Figure S6 (Supporting Information). There is a critical pressure value that depends on the elastic modulus of electrolyte beyond which the shaping effect is observed. Otherwise, applying external pressure fails to work (grey domain). When the elastic modulus of electrolyte ranges from 0.2 to 2.0 GPa, the corresponding critical pressure value increases from 1.2 to 10.0 MPa, which increases almost 10 times. In extreme case of pure liquid electrolyte (the elastic modulus approaches to zero), applying external pressure will always work. Such phase diagram is a useful guide for the pressure management in cell design. Common electrolyte materials are listed in Table S1 (Supporting Information) and visualized in Figure S7 (Supporting Information), including electrolyte immersed separator (Polyolefin and cellulose) and solid polymer electrolyte. For instance, the elastic modulus of a PP separator which usually employed in batteries is about 0.5 GPa.^[29] However, the realistic elastic modulus will be greatly reduced because of the immersion of electrolyte and the existence of porosity.^[30] In that case, applying an external pressure over 1.0 MPa is beneficial for improving the performance of Li metal anodes and the optimal value is no more than 5.0 MPa. It is consistent with experiments carried out by

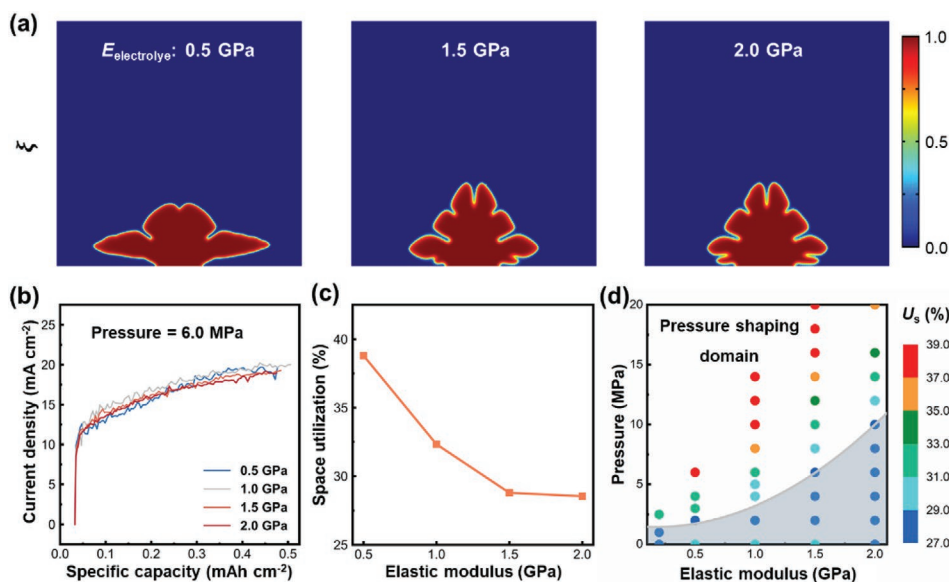


Figure 5. a–c) The pressure shaping effect on the Li dendrite growth in electrolytes of elastic moduli ranging from 0.5 to 2.0 GPa. The applied external pressure is fixed at 6.0 MPa. a) The snapshots of dendritic morphology at a plating capacity of 0.40 mAh cm⁻². b) The current density evolution with the proceeding of electroplating. c) The space utilization in different electrolytes. d) The phase diagram based on the applied external pressure and the elastic modulus of electrolyte at a plating capacity of 0.4 mAh cm⁻². The white region indicates enhanced performance of Li metal anodes, whereas the gray portion denotes that the external pressure fails to work.

Dahn and co-workers. The researchers evaluated anode-free Li metal pouch cells with different external pressures between 75–2205 kPa and proposed an optimal value of 1200 kPa.^[31] Remarkably, the phase diagram presented herein is only applicable to the scenario consistent with the model settings, such as constant voltage (0.10 V, corresponding to an average current density ranging from 10.0 to 20.0 mA cm⁻²) and specific electrolyte properties. The special variations in applied current density (operation condition), ion conductivity (electrolyte), and exchange current density (interface) should be further investigated based on this mechano-electrochemical phase field model. However, the qualitative results on impacts of external pressure are with the same guidance in either case. The optimal value of external pressure in various literatures differs widely.^[31,32] The mechano-electrochemical phase field model conducted herein provides a quantitative approach to design the pressure management system of pouch cells, both in packing and operation.

3. Conclusions

A mechano-electrochemical phase field model was constructed, quantitatively describing the evolution of mechanics, electrochemical reaction, and ion transport in a Li metal battery. With the proposed model and the quantitative analysis, the impacts of the applying external pressure on a pouch cell are revealed: 1) Suppress the proceeding of electroplating reactions (visualized by electrochemical profiles), which is against the rate performance of cells; 2) Promoting the electroplated morphology to be smooth, stocky, and dense (decomposed by the space utilization and the aspect ratio). More specifically, there is a threshold level below which the external pressure fails to work whereas above which the external pressure linearly

improves the performance of Li metal anodes until up to the saturable stage. The side effects of hindering electroplating and causing mechanical instability also determine the selection of optimal pressure. As a concrete reference, a phase diagram of the applied external pressure and the elastic modulus of electrolyte based on special settings is described. Other scenarios can be simulated based on this model and gained quantitatively guiding results. This work gives an essential guidance about why the external pressure should be considered for the practical applications and how it can shape deposited Li and improve the performance of Li metal pouch cells.

4. Experimental Section

Model Formulation: A typical cell, which consists of Li metal electrode and electrolyte (including solid electrolyte and electrolyte-immersed separator), was employed as the research system. The mechano-electrochemical model constructed herein is based on the phase field method proposed by Chen et al.,^[33] except the presence of mechanical field.

Two phases and three components in this system are distinguished by a nonconserved order parameter ξ (electrolyte, $\xi = 0$; Li metal anode, $\xi = 1$) and a concentration set c_i ($i = \text{Li}, \text{Li}^+, \text{and anion}$), respectively. The local electrostatic potential is denoted as ϕ_i ($i = \text{Li}$ and e , represent Li metal electrode and electrolyte, respectively) and the displacement field is represented by \mathbf{u} . The total free energy of this system is given by

$$F = \int_V [f_{\text{grad}}(\xi) + f_{\text{ch}}(\xi, c_i) + f_{\text{elec}}(\xi, c_i, \phi_i) + f_{\text{els}}(\xi, \mathbf{u})] dV \quad (4)$$

where f_{grad} , f_{ch} , f_{elec} , and f_{els} represent the local energy density from the gradient, chemical, electrostatic and elastic contribution, respectively. More specifically, the gradient energy density f_{grad} is expressed by

$$f_{\text{grad}}(\xi) = \frac{1}{2} \kappa_0 [1 + \delta \cos(\omega\theta)] \nabla^2 \xi \quad (5)$$

where κ_0 is the gradient energy coefficient, δ the strength of anisotropy, ω the mode of the anisotropy, and θ the angle between the normal vector of the interface and the reference axis. The chemical and electrostatic energy density can be written as

$$f_{\text{ch}}(\xi, c_i) = g(\xi) + RT \left(c_{\text{Li}^+} \ln \left(\frac{c_{\text{Li}^+}}{c_0} \right) + c_{\text{anion}} \ln \left(\frac{c_{\text{anion}}}{c_0} \right) \right) + \sum c_i \mu_i^\ominus \quad (6)$$

$$f_{\text{elec}}(\xi, c_i, \phi_i) = \sum z_i F c_i \phi_i \quad (7)$$

where μ_i^\ominus is the reference chemical potential of species i , z_i the valence of species i , R the molar gas constant, T the temperature, F the Faraday constant, and $g(\xi)$ the arbitrary double well function: $g(\xi) = W\xi^2(1 - \xi)^2$ with W being the barrier height. The final term f_{els} is expressed by

$$f_{\text{els}}(\mathbf{u}, \xi) = \frac{1}{2} C_{ijkl} \varepsilon_{ij}^E \varepsilon_{kl}^E \quad (8)$$

where ε_{ij}^E denotes the elastic strain tensor, C_{ijkl} the local phase-dependent stiffness tensor:

$$C_{ijkl} = \frac{E}{2(1+\nu)} (\delta_{ij}\delta_{kl} + \delta_{ik}\delta_{jl}) + \frac{E\nu}{(1+\nu)(1-2\nu)} \delta_{ij}\delta_{kl} \quad (9)$$

The electrochemical reaction ($\text{Li}^+ + e^- \rightarrow \text{Li}$) under the driving force of Equation (4) can be deduced from the Butler–Volmer equation. It is expressed by

$$\frac{\partial \xi}{\partial t} = -L_\sigma \left(g'(\xi) + f'_{\text{grad}}(\xi) + f'_{\text{els}}(\mathbf{u}, \xi) \right) - L_\eta h'(\xi) \left(e^{\frac{(1-\alpha)F\eta}{RT}} - \frac{c_{\text{Li}^+}}{c_0} e^{-\frac{\alpha F\eta}{RT}} \right) \quad (10)$$

where L_σ is the interfacial mobility, L_η the reaction constant, α and $1 - \alpha$ the charge-transfer coefficient, c_0 the initial concentration of electrolyte. $h(\xi) = \xi^3(6\xi^2 - 15\xi + 10)$ is an interpolating function. $\eta = \phi_{\text{Li}} - \phi_e - E_{\text{eq}}$ is the overpotential, where ϕ_{Li} denotes the potential of the Li metal anode, ϕ_e the potential of the electrolyte, and E_{eq} the equilibrium potential of electrochemical reaction. The electrochemical reaction is divided into two parts: The front half $(-L_\sigma(g'(\xi) + f'_{\text{grad}}(\xi) + f'_{\text{els}}(\mathbf{u}, \xi)))$ corresponds to the interfacial energy and the second half $-L_\eta h'(\xi) \left(e^{\frac{(1-\alpha)F\eta}{RT}} - \frac{c_{\text{Li}^+}}{c_0} e^{-\frac{\alpha F\eta}{RT}} \right)$ is related to the electrode reaction affinity.

Therefore, the evolution of c_{Li^+} in the electrolyte can be described by the Nernst–Planck equation,

$$\frac{\partial c_{\text{Li}^+}}{\partial t} = \nabla \cdot \left(D_{\text{Li}^+} \nabla c_{\text{Li}^+} + D_{\text{Li}^+} c_{\text{Li}^+} \frac{F}{RT} \nabla \phi_e \right) - c_{\text{Li}^+} \frac{\partial \xi}{\partial t} \quad (11)$$

where D_{Li^+} represents the diffusion coefficient of Li^+ , c_{Li} the initial concentration of electrode. Both diffusion and electromigration are considered.

The electrostatic potential distribution can be expressed by

$$\nabla \cdot (-\sigma_{\text{eff}} \nabla \phi_e) = 0 \quad (12)$$

$$\nabla \cdot (\sigma_{\text{eff}} \nabla \phi_{\text{Li}}) = F c_{\text{Li}} \frac{\partial \xi}{\partial t} \quad (13)$$

Herein, $\sigma_{\text{eff}} = h(\xi) \sigma_{\text{Li}} + (1 - h(\xi)) \sigma_e$ is the effective electric conductivity, where σ_{Li} and σ_e represent the electric conductivity of electrode and electrolyte, respectively.

The mechanical equilibrium equation is given by

$$\nabla \cdot (C_{ijkl} \varepsilon_{kl}^E) = 0 \quad (14)$$

Herein, $\varepsilon_{kl}^E = \varepsilon_{kl}^T - \lambda_i h(\xi) \delta_{ij}$, where ε_{kl}^T is the total strain and λ_i the Vegard strain coefficients. More specifically, $\varepsilon^T = 1/2[(\nabla \mathbf{u})^T + \nabla \mathbf{u}]$. The hydrostatic pressure, principle stress, and von Mises stress were used to visualize the stress evolution.

Model Implementation: This mechano-electrochemical model was simulated by finite element method on COMSOL Multiphysics 5.4. Two-dimensional models with a size of $40 \times 20 \mu\text{m}$ were built in this work. The simulation domain was discretized by triangle mesh at a minimum size of 5 nm and a maximum size of 0.2 μm . Adaptive mesh refinement was

enabled for improving the convergence and accuracy. The voltage between the upper boundary and lower boundary was set as 0.10 V. For 2D model, plain-strain assumption is made. Detailed settings of boundary conditions can be seen in Figure S2 (Supporting Information). The parameters mentioned above are detailed in Table S2 (Supporting Information).

Supporting Information

Supporting Information is available from the Wiley Online Library or from the author.

Acknowledgements

This work was supported by the National Natural Science Foundation of China (21825501 and U1801257), the National Key Research and Development Program (2016YFA0202500 and 2016YFA0200102), and the Tsinghua University Initiative Scientific Research Program.

Conflict of Interest

The authors declare no conflict of interest.

Data Availability Statement

Data available on request from the authors.

Keywords

external pressure, Li dendrites, Li metal batteries, mechano-electrochemical properties, phase field model

Received: October 28, 2020

Revised: December 21, 2020

Published online:

- [1] a) X.-B. Cheng, C.-Z. Zhao, Y.-X. Yao, H. Liu, Q. Zhang, *Chem* **2019**, *5*, 74; b) W. Liu, P. Liu, D. Mitlin, *Adv. Energy Mater.* **2020**, *10*, 2002297; c) R. Xu, X. B. Cheng, C. Yan, X. Q. Zhang, Y. Xiao, C. Z. Zhao, J. Q. Huang, Q. Zhang, *Matter* **2019**, *1*, 317; d) Y. Zhang, T. T. Zuo, J. Popovic, K. Lim, Y. X. Yin, J. Maier, Y. G. Guo, *Mater. Today* **2020**, *33*, 56.
- [2] a) P. R. Shearing, L. R. Johnson, *Joule* **2020**, *4*, 1359; b) P. G. Bruce, S. A. Freunberger, L. J. Hardwick, J. M. Tarascon, *Nat. Mater.* **2012**, *11*, 19; c) Y. X. Lu, X. H. Rong, Y. S. Hu, L. Q. Chen, H. Li, F. L. Chu, F. X. Wu, *J. Energy Chem.* **2020**, *48*, 145; e) X. Shen, H. Liu, X. B. Cheng, C. Yan, J. Q. Huang, *Energy Storage Mater.* **2018**, *12*, 161.
- [3] a) M. Jäckle, A. Groß, *J. Chem. Phys.* **2014**, *141*, 174710; b) B. S. Vishnugopi, F. Hao, A. Verma, P. P. Mukherjee, *Phys. Chem. Chem. Phys.* **2020**, *22*, 11286; c) M. Jäckle, K. Helmbrecht, M. Smits, D. Stottmeister, A. Groß, *Energy Environ. Sci.* **2018**, *11*, 3400.
- [4] D. H. Liu, Z. Bai, M. Li, A. Yu, D. Luo, W. Liu, L. Yang, J. Lu, K. Amine, Z. Chen, *Chem. Soc. Rev.* **2020**, *49*, 5407.
- [5] X. Y. Huang, J. J. Xue, M. Xiao, S. J. Wang, Y. N. Li, S. C. Zhang, Y. Z. Meng, *Energy Storage Mater.* **2020**, *30*, 87.
- [6] a) C. Yan, R. Xu, Y. Xiao, J. F. Ding, L. Xu, B. Q. Li, J. Q. Huang, *Adv. Funct. Mater.* **2020**, *30*, 1909887; b) Y. Xu, H. Wu, H. Jia, J. G. Zhang, W. Xu, C. Wang, *ACS Nano* **2020**, *14*, 8766.

- [7] a) T. Zhang, H. Lu, J. Yang, Z. Xu, J. Wang, S. I. Hirano, Y. Guo, C. Liang, *ACS Nano* **2020**, *14*, 5618; b) S. Park, H. J. Jin, Y. S. Yun, *Adv. Mater.* **2020**, 2002193.
- [8] a) T. Krauskopf, F. H. Richter, W. G. Zeier, J. Janek, *Chem. Rev.* **2020**, *120*, 7745; b) Y. Yamada, J. H. Wang, S. Ko, E. Watanabe, A. Yamada, *Nat. Energy* **2019**, *4*, 269.
- [9] X. Q. Zhang, T. Li, B. Q. Li, R. Zhang, P. Shi, C. Yan, J. Q. Huang, Q. Zhang, *Angew. Chem., Int. Ed.* **2020**, *59*, 3252.
- [10] M. Ue, K. Sakaushi, K. Uosaki, *Mater. Horiz.* **2020**, *7*, 1937.
- [11] S. Sheng, L. Sheng, L. Wang, N. Piao, X. M. He, *J. Power Sources* **2020**, *476*, 228749.
- [12] S. Chen, F. Dai, M. Cai, *ACS Energy Lett.* **2020**, *5*, 3140.
- [13] a) D. P. Wilkinson, H. Blom, K. Brandt, D. Wainwright, *J. Power Sources* **1991**, *36*, 517; b) D. P. Wilkinson, D. Wainwright, *J. Electroanal. Chem.* **1993**, *355*, 193.
- [14] S. Narayan, L. Anand, *Extreme Mech. Lett.* **2018**, *24*, 21.
- [15] X. Zhang, Q. J. Wang, K. L. Harrison, S. A. Roberts, S. J. Harris, *Cell Rep. Phys. Sci.* **2020**, *1*, 100012.
- [16] a) J. W. Tan, A. Cannon, E. Ryan, *J. Power Sources* **2020**, *463*, 228187; b) J. W. Tan, A. M. Tartakovsky, K. Ferris, E. M. Ryan, *J. Electrochem. Soc.* **2016**, *163*, A318.
- [17] a) B. S. Vishnugopi, F. Hao, A. Verma, P. P. Mukherjee, *ACS Appl. Mater. Interfaces* **2020**, *12*, 23931; b) A. Aryanfar, T. Cheng, A. J. Colussi, B. V. Merinov, W. A. Goddard, M. R. Hoffmann, *J. Chem. Phys.* **2015**, *143*, 134701.
- [18] Z. J. Hong, V. Viswanathan, *ACS Energy Lett.* **2018**, *3*, 1737.
- [19] B. S. Vishnugopi, A. Verma, P. P. Mukherjee, *J. Phys. Chem. C* **2020**, *124*, 16784.
- [20] G. Yoon, S. Moon, G. Ceder, K. Kang, *Chem. Mater.* **2018**, *30*, 6769.
- [21] a) A. Jana, S. I. Woo, K. S. N. Vikrant, R. E. García, *Energy Environ. Sci.* **2019**, *12*, 3595; b) J. D. Nicholas, Y. Qi, S. R. Bishop, P. P. Mukherjee, *J. Electrochem. Soc.* **2014**, *161*, Y11.
- [22] a) C. Monroe, J. Newman, *J. Electrochem. Soc.* **2005**, *152*, A396; b) A. Ferrese, J. Newman, *J. Electrochem. Soc.* **2014**, *161*, A1350; c) P. Barai, K. Higa, V. Srinivasan, *Phys. Chem. Chem. Phys.* **2017**, *19*, 20493.
- [23] R. Zhang, X. Shen, X. B. Cheng, Q. Zhang, *Energy Storage Mater.* **2019**, *23*, 556.
- [24] V. Yurkiv, T. Foroozan, A. Ramasubramanian, R. Shahbazian-Yassar, F. Mashayek, *Electrochim. Acta* **2018**, *265*, 609.
- [25] a) L. Q. Zhang, T. T. Yang, C. C. Du, Q. N. Liu, Y. S. Tang, J. Zhao, B. L. Wang, T. W. Chen, Y. Sun, P. Jia, H. Li, L. Geng, J. Z. Chen, H. J. Ye, Z. F. Wang, Y. S. Li, H. M. Sun, X. M. Li, Q. S. Dai, Y. F. Tang, Q. M. Peng, T. D. Shen, S. L. Zhang, T. Zhu, J. Y. Huang, *Nat. Nanotechnol.* **2020**, *15*, 94; b) C. Xu, Z. Ahmad, A. Aryanfar, V. Viswanathan, J. R. Greer, *Proc. Natl. Acad. Sci. U. S. A.* **2017**, *114*, 57.
- [26] Y. Ren, Y. Zhou, Y. Cao, *J. Phys. Chem. C* **2020**, *124*, 12195.
- [27] a) L. Porz, T. Swamy, B. W. Sheldon, D. Rettenwander, T. Frömling, H. L. Thaman, S. Berendts, R. Uecker, W. C. Carter, Y. M. Chiang, *Adv. Energy Mater.* **2017**, *7*, 1701003; b) H. K. Tian, Z. Liu, Y. Z. Ji, L. Q. Chen, Y. Qi, *Chem. Mater.* **2019**, *31*, 7351.
- [28] E. M. Gutman, *Mechanochemistry of Solid Surfaces*, World Scientific Publication, Singapore **1994**.
- [29] a) S. T. Yan, J. Deng, C. Bae, Y. H. He, A. Asta, X. R. Xiao, *Polym. Test.* **2018**, *72*, 46; b) H. M. da Costa, V. D. Ramos, M. G. de Oliveira, *Polym. Test.* **2007**, *26*, 676.
- [30] a) W. G. Xie, W. Y. Liu, Y. P. Dang, A. M. Tang, T. Deng, W. P. Qiu, *J. Power Sources* **2019**, *417*, 150; b) J. Cannarella, X. Liu, C. Z. Leng, P. D. Sinko, G. Y. Gor, C. B. Arnold, *J. Electrochem. Soc.* **2014**, *161*, F3117.
- [31] A. J. Louli, M. Genovese, R. Weber, S. G. Hames, E. R. Logan, J. R. Dahn, *J. Electrochem. Soc.* **2019**, *166*, A1291.
- [32] a) C. F. Zhang, Y. Y. Liu, X. X. Jiao, S. Z. Xiong, J. X. Song, *J. Electrochem. Soc.* **2019**, *166*, A3675; b) C. Fang, B. Lu, G. Pawar, M. Zhang, D. Cheng, S. Chen, M. Ceja, J.-M. Doux, M. Cai, B. Liaw, Y. S. Meng, arXiv:2008.07710 [physics.app-ph] 2020.
- [33] L. Chen, H. W. Zhang, L. Y. Liang, Z. Liu, Y. Qi, P. Lu, J. Chen, L. Q. Chen, *J. Power Sources* **2015**, *300*, 376.